Dynamics of holes and clumps in a mean field Hamiltonian model

D. del-Castillo-Negrete*

Oak Ridge National Laboratory

Oak Ridge TN, 37831-8071

Marie-Christine Firpo

Dipartimento di energetica "Sergio Stecco",

Università degli studi di Firenze,

Via Santa Marta, 3, I-50139 Firenze

Massachusetts Institute of Technology, Cambridge, MA

02139-4307

We study the dynamics and stability of phase space coherent structure evolving self-consistently in a Hamiltonian mean-field model. In plasmas physics the model describes the self-consistent evolution of electron density depletions (holes) and electron density excesses (clumps). In fluids, the model describes the dynamics of vortices with negative (holes) and positive (clumps) circulation in shear flows. We focus on the dynamics of dipolar structures which we describe as two macroparticles. In the macroparticle description we show that the dynamics of symmetric configurations can be described in terms of an integrable nontwist Hamiltonian. A Floquet stability analysis shows that the macroparticle symmetric solution is stable to exponential normal modes but it has a weak algebraic linear instability for asymmetric perturbations. The nontrivial phase space topology of the macroparticle nontwist Hamiltonian leads to bifurcations of the dynamics of the mean field that cause the destruction of dipolar structures and violent mixing of the phase space. Numerical simulations in the $N \to \infty$ kinetic limit and in the finite N case illustrate the stability of weakly asymmetric states and the violent

*e-mail: delcastillod@ornl.gov

mixing.

I. INTRODUCTION

Systems governed by long-range interactions have been shown to develop in some important regimes an effective dynamics controlled by collective modes. Some examples include plasmas physics and stellar dynamics. A convenient way to study these problems is with the use of mean field models in which the many particles interaction is approximated by the interaction of all the particles with an effective potential determined self-consistently from the dynamics of all the particles in the system. In this paper we consider a mean field system known as the single wave model .

In the single wave model in one-dimension, the interaction between N particles and one wave is governed by the Hamiltonian equations

$$\frac{dx_k}{dt} = \frac{\partial \mathcal{H}}{\partial p_k}\,, \qquad \frac{dp_k}{dt} = -\frac{\partial \mathcal{H}}{\partial x_k}\,, \tag{1}$$

$$\frac{d\theta}{dt} = \frac{\partial \mathcal{H}}{\partial J}\,, \qquad \frac{dJ}{dt} = -\frac{\partial \mathcal{H}}{\partial \theta}\,, \tag{2}$$

with Hamiltonian

$$\mathcal{H} = \sum_{j=1}^{N} \left[\frac{1}{2\Gamma_j}\, p_j^2 \; - 2\Gamma_j \sqrt{\frac{J}{N}}\, \cos(x_j - \theta) \right] - UJ \;. \tag{3}$$

The sub-index $k = 1, 2 \ldots N$ labels the particles, U and Γ_k are constant, and x_k are the particle position coordinates with p_k the canonical conjugate momenta. The wave is described by the phase θ and its canonically conjugate variable, the intensity J. Introducing the noncanonical variables

$$a = \sqrt{\frac{J}{N}}\, e^{-i\theta} \;, \qquad u_k = p_k/\Gamma_k \;, \tag{4}$$

the system can be rewritten as

$$\frac{dx_j}{dt} = u_j \,, \tag{5}$$

$$\frac{du_j}{dt} = i\, a(t)\, e^{i\, x_j} - i\, a^*(t)\, e^{-i\, x_j} \tag{6}$$

$$\frac{da}{dt} = iUa + \frac{i}{N} \sum_{j=1}^{N} \Gamma_j\, e^{-ix_j} \,. \tag{7}$$

According to Eqs. (5)-(6) each particle is acted by a single harmonic wave potential with a time dependent amplitude a, whose dynamics is determined by mean-field equation (7). In the kinetic limit ($N \to \infty$), the system is described by a phase distribution function f, evolving according to the Liouville equation

$$\partial_t f + \partial_u H\ \partial_x f - \partial_x H\, \partial_u f\ = 0 \,. \tag{8}$$

where

$$H = \frac{u^2}{2} - a(t)\, e^{i\, x} - a^*(t)\, e^{-i\, x} \,, \qquad \frac{da}{dt} - iUa = \frac{i}{2\pi} \int e^{-ix}\, dx \int du\, f \,. \tag{9}$$

The single wave model model has its origins in the study of the beam plasma instability [1–3]. More recently, the single wave model has been derived under more general conditions to describe the weakly nonlinear dynamics of marginally stable plasmas and shear flows [4,5]. In Ref. [6] the mean field–particle Lagrangian of the model was derived from the full N-body classical mechanics Lagrangian for Coulomb interactions. The single wave model has also been proposed as a reduced model to treat Langmuir turbulence [7] and revisit longstanding basic plasma physics issues, such as the linear [8] and nonlinear Landau damping of a single wave [9]. In a wider context, single wave models have been used to describe a variety of problems including self-consistent Lagrangian transport [10,11], the relationship between self-consistent chaos and phase space coherent structures [12], finite-amplitude non-axisymmetric perturbation of vortices [13], critical layer dynamics in shear flows [14], and free electron lasers [15]. In addition, in the special case when the left hand side of the mean field equation (7) vanishes, the single wave model reduces to the couple rotors Hamiltonian mean field model studied in the context of the statistical mechanics of systems with long-range interactions [16–18].

The model has two constants of motion, the momentum

$$\mathcal{P} = \frac{1}{N}\sum_{j=1}^{N} \Gamma_j \; u_j + |a|^2 \,, \tag{10}$$

and the energy

$$\mathcal{E} = \frac{1}{N}\sum_{j=1}^{N} \Gamma_j \left(\frac{u_j^2}{2} - a\, e^{ix_j} - a^*\, e^{-ix_j} \right) + U\,|a|^2 \,. \tag{11}$$

The parameters Γ_k have a particular significance in the present paper. Previous studies on the single wave model have consider the case $\Gamma_k > 0$ for all k. In fact, early derivations of the model in the plasma physics context consider the problem of the self-consistent interaction of a plasma beam with a compact electron distribution. In this case, only positive Γ_k are acceptable [1,2,6,3]. However, in the description of generic instabilities of marginal stable plasmas it is possible to have positive and negative Γ_k's [4,5,11]. In this case the starting point is a marginally stable background plasma equilibrium density. Perturbations that locally increase the equilibrium density have $\Gamma_k > 0$ and are called "clumps", while perturbations that locally deplete the equilibrium density have $\Gamma_k < 0$ and are called "holes". The study of inhomogeneous structures such as holes and clumps has been of interest in plasma physics [19], fluid dynamics [21] and gravitational systems [20]. As evidenced on expressions (10) and (11), Γ_k formally plays the role of the mass of the point particle k. In the fluid dynamics context, the interpretation of the Γ_k's is straightforward: Γ_k is the circulation of the point vortex k that can be negative or positive.

In a recent paper [12] we discussed preliminary results on the dynamics of symmetric hole-clump coherent structures. In particular, we presented numerical simulations in the finite–N and in the $N \to \infty$ kinetic limit showing the existence of coherent, rotating hole-clump dipole states. The coherence of the dipole was explained in terms of a parametric resonance between the rotation frequency of the dipole and the oscillation frequency of the self-consistent mean field. It was shown that this resonance creates islands of integrability that shield the dipole from regions of chaotic transport. It was also shown that, depending on the initial conditions, the dipole states can be destroyed due to hyperbolic-elliptic bifurcations in the phase space.

The work of in Ref. [12] restricted attention to symmetric hole-clump states. The goal of the present paper is to extend the study of symmetric states discussed in [12], and to study the dynamics of asymmetric hole-clump configurations. In particular, we study in detail the stability of symmetric hole-clump states with respect to asymmetric perturbations.

The organization of the rest of the paper is as follows. Section II presents a discussion of symmetric hole-clump states showing their reduction to a nontwist Hamiltonian, the classification of the topologically different phase space orbits, and the relationship between period and energy. Section III contains a perturbative analysis of $N = 2$ asymmetric states. In particular, we solve the Floquet problem describing the dynamics of perturbed symmetric states, discuss the relationship between the topology of the orbits and the stability of hole-clump states, and show the stability of perturbed shearless orbits. Section IV discusses finite-N and infinite-N kinetic numerical results, and Sec. V presents the conclusions.

II. SYMMETRIC HOLE-CLUMP STATES

A hole-clump dipole sate with N particles is formed by the coherent clustering of $N/2$ holes and $N/2$ clumps. In a first approximation these states can be described as two "macroparticles", one representing the holes and another representing the clumps. In this description, the N particles problem is reduced to a two-particles ($N = 2$) problem. Although in some sense this is a drastic simplification, the two-particles problem is analytically tractable and yields a considerable insight into the dynamics of the N-particle problem. In this section we show that the $N = 2$, symmetric hole-clump problem is fully integrable and discuss the topology of the hole-clump orbits. These results provide an interpretation of the coherence of many-particles hole-clump symmetric states, and will provide the basis of the stability calculations discussed in the next section.

Our starting point is the definition of hole-clump symmetric states. Under the transformation

$$x_k \to x_k - Ut\,, \qquad u_k \to u_k - U\,, \qquad a \to e^{iUt}\,a\,, \tag{12}$$

Eqs. (5) and (6) remain invariant, and Eq. (7) becomes

$$\frac{da}{dt} = \frac{i}{N}\sum_{k=1}^{N} \Gamma_k e^{-i\,x_k} \,. \tag{13}$$

Accordingly, without loss of generality, we can assume that $U = 0$.

When $U = 0$, the single wave model is invariant under the transformation

$$(x_k, u_k, \Gamma_k, a) \longmapsto (-x_k, -u_k, -\Gamma_k, a^*) \,. \tag{14}$$

Initial conditions invariant with respect to this transformation will be called symmetric initial conditions. Since this transformation leaves the equations invariant, this symmetry is conserved for all time. The dynamics of symmetric states involves a smaller number of degrees of freedom than the dynamics of non-symmetric states. In particular, a symmetric state with N particles ($N/2$ holes and $N/2$ clumps) is fully determined by the dynamics of only $N/2$ particles. In addition, for symmetric states $a = a^*$.

According to Eq. (3) a nonsymmetric state with N particles is a $N+1$ degrees of freedom Hamiltonian system. Thus, according to the Liouville-Arnold theorem, $N + 1$ constants of motion are needed for integrability. The only known constants of motion are the energy and the momentum and thus the only known integrable nonsymmetric system corresponds to $N + 1 = 2$, that is a one particle single wave system. This solution was discussed in Ref. [3]. Consideration of hole-clump, symmetric systems opens the possibility of a new family of integrable solution. In fact, a system composed of $N/2$ holes symmetrically opposed in the wave frame to $N/2$ clumps, is effectively an $N/2 + 1$ degrees of freedom system with three constants of motion: the momentum $\mathcal{P}$, the energy $\mathcal{E}$, and the phase of the mean field θ (because $a(t) = a^*(t)$). However, in this case the energy vanishes identically, $\mathcal{E} = 0$, and we only have two constants of motion available, $\mathcal{P}$ and θ, to reduce the number of degrees of freedom. In particular, the system can be integrated in the $N/2 + 1 = 2$ case. That is, the $N = 2$, symmetric, hole-clump system is fully integrable. In the following subsection we describe this solution.

A. Integrability of $N = 2$ states and nontwist Hamiltonian

Consider a two-particle ($N = 2$) symmetric solutions consisting of one clump and one hole with $\Gamma_1 = -\Gamma_2 = \Gamma$, $U = 0$, and symmetric initial conditions $x_1(0) = -x_2(0)$, $u_1(0) = -u_0(0)$, and $a(0) = a^*(0)$. Substituting $x_1(t) = -x_2(t) = x(t)$, $u_1(t) = -u_2(t) = u(t)$ and $a(t) = a^*(t)$ into Eqs. (5)–(7), we get

$$\frac{dx}{dt} = u\,, \qquad \frac{du}{dt} = -2\,a\sin x\ , \qquad \frac{da}{dt} = \Gamma\sin x\,. \tag{15}$$

In this case, the momentum conservation, Eq. (10), reduces to

$$\mathcal{P} = \Gamma u + a^2\,. \tag{16}$$

We will use this conservation law to rewrite Eqs. (15) as an effective one-degree of freedom system. The energy invariant $\mathcal{E}$ in this case is identically zero, and thus cannot be used to reduce the number of degrees of freedom.

For the two-dimensional reduction, we take x and a as basic variables and get u from a using (16). According to (15)-(16), the dynamics in the (x, a) space is governed by the Hamiltonian system

$$\frac{dx}{d\tau} = \frac{\partial H}{\partial A}\,, \qquad \frac{dA}{d\tau} = -\frac{\partial H}{\partial x}\,, \tag{17}$$

with Hamiltonian

$$H = \alpha\,A - \frac{A^3}{3}\ + \cos x\,, \tag{18}$$

where we have introduced the rescaled variables

$$A = a\Gamma^{-2/3}\,, \qquad \tau = \Gamma^{1/3}\,t\,, \qquad \alpha = \mathcal{P}\Gamma^{-4/3}\,. \tag{19}$$

Once A and x are found, u is determined from Eq. (16), namely

$$u = \frac{\mathcal{P}}{\Gamma}\left(1 - \frac{A^2}{\alpha}\right)\,. \tag{20}$$

Being time independent, the Hamiltonian in Eq. (18) is completely integrable. Figure 1 shows contour plots of H =constant, for different values of α. For a given initial condition, $(x(0), A(0))$, the orbit simply follows the corresponding $H = H(0)$ contour. As observed in the plots, when $\alpha < 0$ the system (17) has no fixed points, and when $\alpha > 0$ the system has four fixed points: $(x_0, A_0) = (0, \sqrt{\alpha})$, $(0, -\sqrt{\alpha})$, $(\pi, \sqrt{\alpha})$, and $(\pi, -\sqrt{\alpha})$, with eigenvalues $\lambda = \pm i\omega$, $\lambda = \pm\omega$, $\lambda = \pm\omega$, and $\lambda = \pm i\omega$, respectively, where

$$\omega = \sqrt{2}\alpha^{1/4}\,. \tag{21}$$

Note that, because the equations of motion (17) are invariant under the transformation $(x, A) \longmapsto (x + \pi, -A)$, the elliptic and hyperbolic fixed points come in pairs. The value $\alpha = 0$ is the bifurcation point at which an elliptic-hyperbolic doublet is created at $x = 0$, and another elliptic-hyperbolic doublet is created at $x = \pm\pi$.

One-degree of freedom Hamiltonians of the form $H(q, p) = p^2/2 + V(q)$, are typically non-degenerate in the sense that, when transformed to action angle variables $H = H(J)$, the frequency, $\omega = \partial_J H$, is a *monotonic* function of the action. That is, $\partial_J^2 H \neq 0$. However, there are situations in which the Hamiltonian is degenerate in the sense that $\partial_J^2 H = 0$ for a specific value of the action, $J = J_*$. When this is the case, the Hamiltonian is called *nontwist*. In recent years, it has been realized that nontwist Hamiltonians appear in many areas including chaotic advection in fluids, stochasticity of magnetic field lines in plasmas, celestial mechanics, accelerator physics, and atomic physics among others. Because of the degeneracy, many well-know powerful theorems and results, including the celebrated KAM (Kolmogrov-Arnold-Moser) theorem, can not be applied to nontwist systems (for further discussion see for example Ref. [22] and reference therein). The reduced Hamiltonian of the symmetric dipole in Eq. (18) has the canonical form of a nontwist Hamiltonian in the (x, A) variables.

B. Separatrix reconnection and orbits topology

One of the main signatures of nontwist Hamiltonians is that they exhibit global changes in the phase space topology known as *separatrix reconnection* [23,22]. The change in the phase space topology observed in panels (b), (c) and (d) of Fig. 1 is an example of separatrix reconnection and it involves the different ways in which the stable and unstable manifolds of the hyperbolic fixed points can be connected. There are two separatrices: the upper branch which emanates from the hyperbolic point at $(\pm\pi, \sqrt{\alpha})$ and the lower branch that emanates from the hyperbolic point at $(0, -\sqrt{\alpha})$. The topology in panel (b) of Fig. 1 is known as the *homoclinic* topology and the one in panel (d) is known as the *heteroclinic* topology. Panel (c) shows the separatrix reconnection threshold. The reconnection threshold can be computed by observing that at the reconnection point $H(P_0) = H(P_\pi)$, where H is the Hamiltonian in Eq. (18), $P_0 = (0, -\sqrt{\alpha})$, and $P_\pi = (\pi, \sqrt{\alpha})$. This condition gives the reconnection threshold

$$\alpha_* = (3/2)^{2/3}\,. \tag{22}$$

For $\alpha < \alpha_*$ the Hamiltonian has the homoclinic topology, and for $\alpha > \alpha_*$ it has the heteroclinic topology. For further discussion on separatrix reconnection and nontwist Hamiltonians see [22], and references therein.

Using the definition of α in (19) we have the following condition for reconnection in terms of the total momentum of the system $\mathcal{P}$ and the value of Γ:

$$\mathcal{P} < \left(\frac{3\,\Gamma^2}{2}\right)^{2/3} \quad \text{Homoclinic}\,, \qquad \mathcal{P} > \left(\frac{3\,\Gamma^2}{2}\right)^{2/3} \quad \text{Heteroclinic}\,, \tag{23}$$

with $\mathcal{P} = (3\,\Gamma^2/2)^{2/3}$ giving the reconnection threshold.

The orbits in the (x, A)–phase space can be classified in three groups: trapped orbits, untrapped orbits, and separatrix orbits. To each one of these orbits corresponds an orbit in the (x, u)-phase space. Figures 2–4 show orbits in the (x, u)–space corresponding to the different topologies in the (x, A) –space, with $\mathcal{P}/\Gamma = 1$. In these plots, orbits corresponding to holes are shown with dashed curves and those corresponding to clumps are shown with

solid curves. The panels (a) and (d) of Figures 2–4 are particularly interesting because they illustrate how the changes in the phase space topology due to separatrix reconnection in the (x, A) space gives rise to changes in the topology of separatrix and untrapped orbits in the (x, u)-phase space.

C. Shearless orbit

As mentioned before, in a nontwist Hamiltonian, $\partial_J^2 H = 0$ for a specific value of the action, $J = J_*$. The orbit with $J = J_*$ is known as *shearless* orbit, and it plays an important role in the study of nontwist systems. For example, in the absence of separatrix reconnection, the shearless orbit is typically the most robust KAM curve when the Hamiltonian is perturbed with a non-integrable, time-periodic perturbation [22]. In this subsection we find the condition defining the shearless orbit in the Hamiltonian in Eq. (17). This result will be used in the next section where we discuss the stability of symmetric hole-clump states that correspond to shearless orbits of the reduced nontwist Hamiltonian. We will restrict attention to the heteroclinic topology and consider untrapped orbits between the lower and upper branches of the separatrices. With respect to Fig. 1-(d), we consider orbits with initial conditions around $(x_0, A_0) \approx (-pi, 1)$.

Integrating the equation for $dx/d\tau$ in (17) we obtain

$$T = \int_0^T d\tau = \int_{-\pi}^{\pi} \frac{dx}{\alpha - A^2(H, x)}\,, \tag{24}$$

where A is determined as function of x and the energy H by solving the cubic equation $H = \alpha A - A^3/3 + \cos x$, and taking the root that corresponds to the initial condition under consideration (i.e. the one between the two separatrices in the heteroclinic topology). Taking the derivative of Eq.(24) with respect to H and changing the independent integration variable using $dx = \dot{x}(t)dt = (\alpha - A^2(t))\, ds$ we obtain

$$\frac{\partial T}{\partial H} = \int_{-\pi}^{\pi} \frac{2A(t)}{[\alpha - A(t)]^2}\, dt\,. \tag{25}$$

The shearless orbit is the one for which $\partial_J \omega = 0$ and this corresponds to $\partial_H T = 0$ because $T = 2\pi/\omega$ and $\omega = \partial_J H$ imply $\partial_J \omega = -(4\pi^2/T^3)\,\partial_H T$.

III. PERTURBATIVE ANALYSIS OF $N = 2$ ASYMMETRIC STATES

One of the main goals of the present paper is the study of asymmetric dipolar states. That is, states which are not invariant with respect to the transformation in Eq. (14). In the macroparticle description this problem corresponds to the study of the $N = 2$ single wave model for asymmetric initial conditions. The lack of symmetry introduces several technical difficulties. In particular, in this case the wave-particle phase space is six dimensional and a reduction to a low-degree of freedom integrable Hamiltonian system does not seem in general possible, because, to our knowledge, the system has no more constants of motion in addition to the energy and the momentum. Numerical simulations in this case show the existence of regular and chaotic trajectories. The regular orbits are the one of particular interest here because they are likely candidates for coherent structures in the macroparticle description. As a first step in the understanding of this complex problem we limit attention to weakly asymmetric states. That is, we study the evolution of initial conditions in the vicinity of symmetric solutions.

This problem is related the stability of symmetric solutions with respect to small perturbations. As discussed in the previous section, the configuration formed by one macroparticle representing a clump with $\Gamma_1 = \Gamma > 0$, symmetrically opposed in the wave reference frame to a macroparticle representing a hole with $\Gamma_2 = -\Gamma$, is an integrable solution. In the macroparticle description, this configuration represents a coherent structure and an important dynamical issue consists in testing its robustness. For that matter, we study here the stability of the hole-clump dipolar structure with respect to small perturbations. We consider the dipolar hole-clump two-particle system given by Eq. (15). This is a special solution of Eqs. (5)–(7) and we study the temporal evolution of small deviations to it.

A. Floquet analysis of linearized equations

Let us first write down the equations of motion of the particles $i = 1, 2$ and of the wave variables in terms of the new variables introduced in (19). We put $U = 0$ and define $v_i = \Gamma^{-1/3} u_i$ as well as X and Y, the Cartesian coordinates of the wave, that is $X = |A| \cos\theta$ and $Y = |A| \sin\theta$. In this notation, the equations of motion (5)–(7) become

$$\begin{aligned} \frac{dx_i}{d\tau} &= v_i \\ \frac{dv_i}{d\tau} &= -2\left(X \sin x_i - Y \cos x_i\right) \\ \frac{dX}{d\tau} &= \frac{1}{2}\left(\sin x_1 - \sin x_2\right) \\ \frac{dY}{d\tau} &= \frac{1}{2}\left(\cos x_1 - \cos x_2\right) \end{aligned} \tag{26}$$

Let $x_{1d}(t) \equiv x_d(t)$, $x_{2d}(t) = -x_d(t)$, $v_{1d}(t) \equiv v_d(t)$, $v_{2d}(t) = -v_d(t)$ and $X_d(t) = A_d(t)$, $Y_d(t) = 0$ be a solution of the equations of motion of the symmetric hole-clump pair. That is, $x_d(t)$ and $A_d(t)$ satisfy the Hamiltonian equations of motion (17). Substituting $x_1 = x_d + \delta x_1$, $x_2 = -x_d + \delta x_2$, $v_1 = v_d + \delta v_1$, $v_2 = -v_d + \delta v_2$ and $X = A_d + \delta X$, $Y = \delta Y$ into Eq. (26) and neglecting nonlinear terms, we get

$$\frac{d\delta x_1}{d\tau} = \delta v_1$$

$$\frac{d\delta x_2}{d\tau} = \delta v_2$$

$$\frac{d\delta v_1}{d\tau} = -2A_d \cos x_d \delta x_1 - 2\sin x_d \delta X + 2\cos x_d \delta Y$$

$$\frac{d\delta v_2}{d\tau} = -2A_d \cos x_d \delta x_2 + 2\sin x_d \delta X + 2\cos x_d \delta Y$$

$$\frac{d\delta X}{d\tau} = \frac{1}{2}\cos x_d \left(\delta x_1 - \delta x_2\right)$$

$$\frac{d\delta Y}{d\tau} = \frac{1}{2}\sin x_d \left(\delta x_1 + \delta x_2\right).$$

Introducing the center of mass position $z_1 = (x_1 + x_2)/2$ and momentum $p_1 = (v_1 + v_2)/2$, and the relative coordinates $z_2 = (x_1 - x_2)/2$ and $p_2 = (v_1 - v_2)/2$ enables to break the previous system in two decoupled systems of three first-order ordinary differential equations

$$\frac{d}{d\tau}\begin{pmatrix}\delta z_1\\ \delta p_1\\ \delta Y\end{pmatrix} = \begin{bmatrix}0 & 1 & 0\\ -2A_d\cos x_d & 0 & 2\cos x_d\\ -\sin x_d & 0 & 0\end{bmatrix}\begin{pmatrix}\delta z_1\\ \delta p_1\\ \delta Y\end{pmatrix}. \tag{27}$$

and

$$\frac{d}{d\tau}\begin{pmatrix}\delta z_2\\ \delta p_2\\ \delta X\end{pmatrix} = \begin{bmatrix}0 & 1 & 0\\ -2A_d\cos x_d & 0 & -2\sin x_d\\ \cos x_d & 0 & 0\end{bmatrix}\begin{pmatrix}\delta z_2\\ \delta p_2\\ \delta X\end{pmatrix}. \tag{28}$$

As $x_d(t)$ and $A_d(t)$ are time-periodic solutions, the systems (27) and (28) amount to a Floquet problem. As we are interested in systems where holes and clumps are initially symmetric with respect to the wave frame, the center of mass system (27) is identically zero and we will only focus on the second system (28). This is just the linearization of the equations of motion of the integrable dipole solution, with $\delta A = \delta X$. We will see that this fact has important consequences on the stability. The linearization of the total momentum

$$\tilde{\mathcal{P}} = \delta p_2 + 2A_d\delta X = \Gamma^{-4/3}\,\delta\mathcal{P} \tag{29}$$

is constant under the evolution (28). Let us define $\boldsymbol{\phi}(\tau) = (\delta z_2(\tau), \delta X(\tau))$, $\mathbf{b} = \left(\tilde{\mathcal{P}}, 0\right)$ and

$$A(\tau) = \begin{bmatrix}0 & 2A_d\\ -\cos x_d & 0\end{bmatrix} \tag{30}$$

that is a time-periodic matrix. Using the constant (29), the stability problem reduces to the study of the two-dimensional system

$$\dot{\boldsymbol{\phi}} + A(\tau)\,\boldsymbol{\phi} = \mathbf{b}. \tag{31}$$

Let $M(\tau)$ denote a fundamental T-periodic homogeneous solution matrix of (31), that is a matrix whose columns are linearly independent solutions of system (31) with zero right-hand side. Then, using the variation-of-constant formula, the solution $\boldsymbol{\phi}$ of (31) is

$$\boldsymbol{\phi}(\tau) = M(\tau)\,\boldsymbol{\phi}(0) + M(\tau)\int_0^\tau M^{-1}(s)\,\mathbf{b}ds. \tag{32}$$

The stability properties are given by the homogeneous system with $\mathbf{b} = \mathbf{0}$. To solve this problem, we first note that according to Eq. (17)–(18).

$$\boldsymbol{\phi}_1 = \begin{pmatrix} \dot{x}_d \\ \dot{A}_d \end{pmatrix} = \begin{pmatrix} \alpha - A_d^2 \\ \sin x_d \end{pmatrix} \tag{33}$$

is a solution of the homogeneous Floquet system. As $\boldsymbol{\phi}_1$ is periodic, it is associated with a Floquet multiplier equal to one. A basis of solutions can be completed by another linearly-independent solution

$$\boldsymbol{\phi}_2 = \begin{pmatrix} u_2 \\ v_2 \end{pmatrix} \tag{34}$$

such that the Wronskian, that is the determinant of the fundamental matrix, $\det M$, does not vanish. In general $\det M$ is a function of time. However, for the system under consideration $\det M$ is a constant, which without loss of generality we can take equal to one:

$$\det M = \dot{x}_d v_2 - \dot{A}_d u_2 = 1\,. \tag{35}$$

To show this we use the use the fact that $M' = -A\,M$ implies $(\det M)' = -(\mathrm{Tr}\,A)\,(\det M)$ where the primes denote derivative with respect to time. Integrating this last equation yields $\det M(\tau) = \det M(0)\,\exp\int_0^\tau \mathrm{Tr}\,A$. In this case $\mathrm{Tr}\,A = 0$ which implies $\det M(\tau) = \det M(0)$.

According to Eqs. (33)-(34), the solution of the homogeneous system associated to (32) is then $\boldsymbol{\phi}(\tau) = M(\tau)\,\boldsymbol{\phi}(0)$ where

$$M(\tau) = \begin{bmatrix} \alpha - A_d^2(\tau) & u_2(\tau) \\ \sin x_d(\tau) & v_2(\tau) \end{bmatrix} \begin{bmatrix} v_2(0) & -u_2(0) \\ -\sin x_d(0) & \alpha - A_d^2(0) \end{bmatrix}, \tag{36}$$

where Eqs. (33)-(34) were used. Moreover, according to the linear independence condition (35), u_2 and v_2 are the solutions of

$$\dot{x_d}\,\dot{u_2} = -2A_d\left(1 + \dot{A}_d\,u_2\right)\,, \qquad \dot{A}_d\,\dot{v_2} = \cos x_d\;(\dot{x_d}v_2 - 1)\;. \tag{37}$$

If T denotes the period of the dipole integrable solution, then $M(T)$ is the one-period time advance solution of the homogeneous problem. Using (35) it is straightforward to show that ϕ_1 is an eigenvector of $M(T)$ with eigenvalue $\lambda_1 = 1$. On the other hand, again from (35) it follows that $\det M = 1$ and therefore the product of the eigenvalues of M is one, $\det M = \lambda_1\lambda_2 = 1$. From here we conclude that $\lambda_2 = 1$. That is, $M(T)$ has two degenerate eigenvalues equal to one.

It can be shown, solving the full system (32), that the infinitesimal perturbations δz_2 and δX are growing within two linear functions of time. Let us consider for instance the evolution of δz_2. Assuming $\tilde{\mathcal{P}} = 0$ and $\delta X(0) = 0$ in order to get simple expressions, we obtain from (32)

$$\delta z_2\,(\tau + T) - \delta z_2\,(\tau) = T g\,(\tau)\sin x_d(0)\delta z_2\,(0)$$

with

$$g\,(\tau) = -\frac{u_2(\tau + T) - u_2(\tau)}{T}. \tag{38}$$

Provided T is finite, which excludes perturbations around separatrices, it is easy to check using (37) that $g\,(\tau)$ is a time-dependent function of period T. Therefore the perturbation $\delta z_2\,(\tau)$ is bounded by a linear envelope of slope γ given by

$$\gamma = \max_{0\le\tau\le T}\frac{\delta z_2\,(\tau + T) - \delta z_2\,(\tau)}{T} = \left|\sin x_d(0)\delta z_2\,(0)\right| \max_{0\le\tau\le T} g\,(\tau)\,. \tag{39}$$

It should be noted that, as apparent on (39), the numerical value of γ depends on the initial perturbation. This result shows that the dipole solution, except possibly motions along the separatrices, is linearly stable, in the sense that small perturbations do not grow exponentially. However, perturbations are not bounded and their envelope grows linearly with time. We shall use below the expression of γ in Eq. (39) as an indicator of the rate to enter the nonlinear regime.

B. Bifurcation in the homoclinic topology

In order to study the stability of system (28) in terms of the problem parameters, we consider here the solutions $(x_d(t), A(t))$ associated to the following class of initial conditions: we take $x_d(0) \equiv x_0 \neq 0$ and $v_d(0) = 0$, which according to (19) brings the simple relation

$$\alpha = A_0^2. \tag{40}$$

Varying the initial wave amplitude is then directly equivalent to playing with the parameter α. We shall take $x_0 = 0.3$ and $A_0 = \sqrt{\alpha} > 0$ to fix ideas. This means that we consider initially a dipole close to the bottom of the wave trough. The energy of the dipole solution is given by $H(A_0, x_0)$, that is, using (18),

$$H(A, x) = \alpha A - \frac{A^3}{3} + \cos x = \left(\frac{\alpha}{\alpha_*}\right)^{3/2} + \cos x_0. \tag{41}$$

The phase space plots associated to this class of initial conditions only evolve in the homoclinic topology framework, as depicted in Fig. 1-(b).

The trajectories in (x, A) space associated to (41) undergo a topological bifurcation for a critical value of α, that we denote by α_c. In (x, A) space, for α below α_c the trajectory is a passing one. As α increases, approaching α_c this trajectory constricts and eventually the left and right branches around the $x = 0$ axis touch in a singular point at α_c. Above α_c, the phase space plots associated to (41) show two disconnected paths, associated to one passing and one trapped trajectories. For the initial data considered here, the dipole solution corresponds to the trapped trajectory in (x, A) space. This transition may be easily derived by noting that the expression (41), applied to $x = 0$, is a polynomial of third order in A. For $\alpha < \alpha_c$, $H(A, 0) = H(A_0, x_0)$ admits a single real solution for A. At the bifurcation point $\alpha = \alpha_c$, this third order polynomial form in A has, in addition to this single root, another double real root that looses its degeneracy when $\alpha > \alpha_c$. Using this property, one obtains the threshold

$$\alpha_c = \alpha_* \left(\frac{1 - \cos x_0}{2}\right)^{2/3}. \tag{42}$$

In our case ($x_0 = 0.3$), which corresponds to the numerical value $\alpha_c \simeq 0.103914$.

We numerically computed the time period of system (41) as a function of α. The result is plotted on Fig. 5. For large values of α, we note that the period of the dipole solution converges to the rotation period around the wave trough elliptic point, that is $T = 2\pi/\omega = \sqrt{2}\pi\alpha^{-1/4}$, where ω is defined in (21), and coincides therefore with the trapping frequency at the bottom of the pendulum potential (5)-(6). This fact will be relevant for the stability study. At α_c, the period diverges which signals the separatrix orbit.

Fig. 6 shows a computation of the product γT –which represents the maximal change in δz_2 over one period– as a function of α for a vanishing $\tilde{\mathcal{P}}$ and $\delta z_2(0) = 0.01$. The features apparent in this figure generalize to arbitrary initial perturbations. It is clear that, for α below α_c, the linear analysis breaks on a time scale that is shorter (or of the order of) one period of the dipole system since γT is of order one and even diverges as α tends to α_c. For α above α_c, the value of γT drops dramatically and, for sufficiently large α, the linear analysis will have a long-time validity, meaning that small perturbations of the dipole solution will approach the latter one during many rotation periods.

The relatively high value reached by γT below α_c is due to the roughly exponential growth stage experienced by the perturbation within a fraction of the period T. In the (x, A) space, this occurs when the reference integrable dipole trajectory constricts and bends as it approaches the x-point. In the (x, v) representation, the reference integrable solution exhibits then 'festoon'-like patterns, as the one plotted in Fig. 2 for $\alpha < \alpha_c$, that is a topology very inconsistent with the integrable pendulum one. This stage signals the degeneracy in the v-representation, that we remind is not a canonical variable here. This temporarily exponentially unstable behavior experienced by a perturbed dipole is sufficient to bring any initially small perturbation to the integrable solution up to order $\mathcal{O}(1)$ and even large values breaking the linear regime. This will be illustrated in a more dramatic way on finite-N simulations. If one adds then a non-symmetric perturbation, that is if $\delta z_1(0)$ or $\delta Y(0)$ in system (27) are non-vanishing then the system will evolve so as to remove this degeneracy and suppress elliptic-hyperbolic bifurcations of the wave trough.

For α larger than α_c, the time scale to enter the nonlinear regime is however strongly decreased. This occurs when the topology of the reference trajectories is isomorphous to the pendulum one. There is still another threshold remaining at a value α_0 above α_c. This is associated to the elliptic-hyperbolic bifurcation of the wave trough, as described in paragraph II B. Below α_0, the sign of the wave amplitude A is not constant in time. One obtains easily, for the initial conditions considered here

$$\alpha_0 = \alpha_* \left(1 - \cos x_0\right)^{2/3} = 2^{2/3}\alpha_c. \tag{43}$$

Its numerical value is 0.165. Yet this threshold is not spectacular here as it does not coincide with the approach of the x-point in the (x, A) space.

C. Stability of shearless orbits

In this subsection we discuss the stability properties of symmetric dipole solutions corresponding to shearless orbit in the (x, A) space of the reduced nontwist Hamiltonian. Without loss of generality we assume that $u_2(0) = 0$ in Eq.(36). Then, according to linear independence condition in Eq. (35), $v_2(0) = 1/\dot{x_d}(0)$. We will focus in the heteroclinic topology case, $\alpha > \alpha_* = (3/2)^{2/3}$, and consider initial conditions with $x_d(0) = 0$, $A_d(0) \in (A_{min}, A_{max})$ where A_{min},, and A_{max} delimit the orbits between the lower and upper separatrices. For these initial conditions, the solution of Eqs. (37) gives

$$u_2(\tau) = \left[\frac{u_2(0)}{\dot{x_d}(0)} - F(\tau)\right] \dot{x_d}(\tau)\,, \tag{44}$$

$$v_2(\tau) = \frac{1}{\dot{x_d}(\tau)} + \left[\frac{u_2(0)}{\dot{x_d}(0)} - F(\tau)\right] \dot{A}_d(\tau)\,, \tag{45}$$

with

$$F(\tau) = \int_0^\tau \frac{2\,A_d}{\left(\alpha - A_d^2\right)^2}\, ds\,. \tag{46}$$

Accordingly, the change in δz_2 and δX over one period T is

$$\delta z_2(T+\tau) - \delta z_2(\tau) = -\left[\alpha - A_d^2(0)\right]\,\left[\alpha - A_d^2(\tau)\right]\,\delta X(0)\,\frac{\partial T}{\partial H}\,, \tag{47}$$

$$\delta X(T+\tau) - \delta X(\tau) = -\left[\alpha - A_d^2(0)\right]\,\delta X(0)\,\sin x_d(\tau)\,\frac{\partial T}{\partial H}\,, \tag{48}$$

where we have use Eq. (25). That is, weakly asymmetric initial conditions separate from the symmetric solutions, linearly in time, and the rate of separation is proportional to the derivative of the rotation period T with respect to the energy of the initial condition $H = \alpha A_d(0) - A_d^3(0)/3 + 1$. According to the discussion in Sec. II-C, for a shearless orbit

$$\frac{\partial T}{\partial H} = 0\,, \tag{49}$$

and thus we conclude that symmetric hole-clump dipole structures corresponding to shearless orbits are stable.

To illustrate this ideas we integrated the single wave model for $N = 2$, $\Gamma_1 = -\Gamma_2 = 1$, $U = 0$ and

$$x_1(0) = x_2(0) = 0 \qquad u_1(0) = [\alpha - A_d^2(0)] - 4\,\varepsilon\,A_d^2(0)\,, \qquad u_2(0) = -[\alpha - A_d^2(0)]\,. \tag{50}$$

$$a_R(0) = (1+\varepsilon)\,A_d(0)\,, \qquad a_I(0) = 0\,, \tag{51}$$

with $\alpha = 1.95$, $A_d(0) = -0.5397$, $\varepsilon = 0.1$. These initial conditions correspond to an order ε asymmetric perturbation of the symmetric hole-clump solution x_d, u_d, A_d. To see this, recall that according to Eq. (19), for $\Gamma = 1$, $a = A$ and $\alpha = \mathcal{P}$, where $\mathcal{P} = u(0) + a^2(0)$ is the total momentum. The value of α was chosen to be 1.95 in order to have the heteroclinic topology in the (x, A) non-twist reduced Hamiltonian, and the initial condition of $A_d(0)$ was chosen so that the symmetric dipole is the shearless dipole. That, is $\partial_T H = 0$.

Figure 7 shows the phase space orbits of the hole and clump. The dashed lines denote the unperturbed shearless dipole (x_d, u_d), and the solid lines the perturbed orbit. As expected, due to the stability properties of the shearless dipole, the neighboring trajectory stay close to the shearless orbit. Figure 8 shows the real and imaginary parts of the mean field created

by the perturbed hole-clump system. In the absence of perturbation, the mean field would be single periodic with $a_I - 0$ for all t. The asymmetric perturbation yields to a quasiperiodic time dependence and a finite a_I.

IV. NUMERICAL RESULTS

In this section we present results obtained form the numerical integration of the single wave model in the kinetic limit and in the finite $N \gg 1$ case.

A. Kinetic simulations

The existence of clustered states corresponding to symmetric, dipolar distribution of holes and clumps was studied in Ref. [12]. As discussed before, the symmetric system has the advantage of having an extra conservation law, and an important issue is to explore whether or not coherent states can exists when the symmetry condition is relaxed. The dynamics of asymmetric initial conditions is quite rich, and it is in general not integrable even in the $N = 2$ case. However, here we show numerical evidence that it is possible to have asymmetric coherent states in the kinetic limit.

We consider an initial condition of the form

$$f(x,u,t=0) = \sum_{j=1}^{2} \gamma_j \, \exp\left[-\left(\frac{x-x_j}{\sigma_x}\right)^2 - \left(\frac{u-u_j}{\sigma_u}\right)^2 \right], \qquad a(t=0) = a_0\,, \tag{52}$$

with $\gamma_1 = -\gamma_2 = 11.11$, $x_1 = x_2 = \pi$, $\sigma_x = 0.3$, $\sigma_u = 0.3$, and $U = 0$.

$$u_1 = \alpha - a_0^2 - 4\,\varepsilon\, a_0^2\,, \qquad u_2 = \alpha - a_0^2 \tag{53}$$

where $\varepsilon = 0.1$, $a_0 = -0.5397$, $\alpha = 1.95$. This initial condition corresponds to the $N = 2$ initial condition (50)-(51) discussed in Sec. III-c. That is, in the macroparticle description, this initial condition corresponds to a weakly asymmetric shearless dipole. Figure 9 shows the evolution of the distribution function f the phase space. Contrary to the symmetric case discussed in Ref. [12], the center of mass of the dipole drifts, but the dipole retains

its coherence and the relative distance between the hole and the clump remains bounded. This results are a direct consequence of the stability analysis discussed in the previous sections. Figure 10 shows the dynamics of the mean field. Consistent with the macroparticle description, the mean field shows a quasiperiodic time evolution similar to the one observed in the $N = 2$ case.

B. Finite-N simulations of initially trapped, symmetric hole-clump structures

We wish now to test the stability of the hole-clump coherent structure by performing finite-N simulations relevant to the class of initial conditions studied in paragraph III B. We use the fourth-order symplectic algorithm presented in Ref. [24] for the self-consistent wave-particle Hamiltonian, suitably modified to account for the two species of particles. Instead of considering only one (macro) clump and one (macro) hole, we consider initially two patches of holes and clumps having a small extension in the phase space. We put, without loss of generality $U = 0$ and $\theta(0) = 0$. In the simulations, N particles with positive Γ are uniformly distributed around an average zero velocity $v_0 = 0$ in the wave referential and position $x_0 = 0.3$ with indices $1 \leq i \leq N$. They are symmetrically opposed to N particles having a negative mass $-\Gamma$ and indices $N + 1 \leq i \leq 2N$. To create a dipolar structure, one puts $\forall i = 1, \ldots, N$,

$$x_i(0) = -x_{i+N}(0). \tag{54}$$

This ensures that, up to numerical errors, any hole-clump pair within the two bunches of symmetrically opposed holes and clumps remains symmetric in the wave frame for all time. The remaining free parameter is the initial wave amplitude $A_0 > 0$. This is associated to the natural velocity scale of the problem, which is of the order of the initial total width in velocity of the wave resonance, that is $4\sqrt{2A_0} = 4\omega$. This induces us to rescale both initial bunches of holes and clumps in the phase space (x, v) along the velocity axis so that the extension in velocity of the patches is a constant fraction of $\sqrt{A_0}$. In this way, all the

initial phase spaces are identical in the rescaled variables $(x, v/\omega)$. In these dimensionless coordinates, the initial uniform patches we consider are disks of radius $r_0 = 0.05$. We then study the stability of these initial dipolar structures as a function of A_0. Referring to the two-macroparticles hole-clump description in Eqs. (17)-(19), these initial conditions fix α through Eq. (40), which determines the momentum $\mathcal{P}$ of the system, and the energy H through Eq. (41). Using these initial conditions will enable us to compare results from these finite-N simulations with the analytical derivations of the previous Section. In particular, in Sec. III-B it was observed that in the homoclinic topology, the $N = 2$ orbits exhibit a topological bifurcation for a critical value $\alpha = \alpha_c \approx 0.103914$. To explore the effect of this bifurcation in the finite $N \gg 1$ case, we integrated the model for $\alpha = 0.056$, 0.1, 0.13 and 0.206.

To measure the spatial coherence of the dipole structure, that is its stability in the center-of-mass reference frame, we introduce the 'order parameter'

$$\mathbf{M}_d = \left(\frac{1}{N} \sum_{i=1}^{N} \cos\left(x_i\right), \frac{1}{N} \sum_{i=1}^{N} \sin\left(x_i\right) \right). \tag{55}$$

At initial time, $\|\mathbf{M}_d\|$ is almost equal to 1, indicating a clustered state. An homogeneous repartition of holes (and consequently of clumps) would correspond to $\|\mathbf{M}_d\| = \mathcal{O}\left(N^{-1/2}\right)$ according to the central limit theorem. We use then this parameter as an indicator of the ability of the system to sustain a dipole-like coherent structure.

Several numerical simulations were performed varying the control parameter $X_0 = A_0$, or equivalently α. In Fig. 11 we plot the evolution of the norm of the order parameter $\mathbf{M}_d$ for some values of α. For the same values of α, the time evolution of the Cartesian coordinates of the wave X and Y are plot on Fig. 12. The Y curves remain almost vanishing during all the runs in agreement with the symmetry constraint (implying $a = a^*$). Because of unavoidable numerical errors the center-of-mass system (system (27) in the 2-particle model) is eventually destabilized. This is a large-time phenomenon that basically does not affect much the dynamical observations: when it takes place, the coherent structure has already been violently scattered as in Fig. 13 if α is small enough or continues to rotate

coherently in the vicinity of the wave trough, as shown on Fig. 14 due to parametric effects. *give an estimate of the impact of parametric effects - function of the radius of the structure* -

V. SUMMARY AND CONCLUSION

Coherent structures are ubiquitous in plasmas, fluids and dynamical systems in general. These structures have been observed in experiments and numerical simulations, and there has been a considerable effort in trying to understand them. A problem complementary to the formation of coherent structures is the problem of "violent" mixing and relaxation of far from equilibrium initial conditions. By violent mixing we mean a phase space mixing process with a time scale faster than diffusion or even chaotic advection. In the present paper we have discussed these two problems in the context of a simplified model known as the single wave model. The single wave model is a Hamiltonian mean field model that describes the weakly nonlinear dynamics of marginally stable fluids and plasmas. Due to its mean field nature, the model fall in the category of systems with long-range interaction, that have recently attracted significant interest due to their intriguing statistical mechanics behavior.

In a previous paper, [12], we showed the existence of coherent structures associated with symmetric states and explained their resilience in the context of self-consistent chaos. One of the goals of the present paper was to extend these results to the case of non-symmetric states. The relaxation of the symmetry condition introduces several technical difficulties. For example, the $N = 2$ asymmetric case does not seems to be integrable. To gain some understanding into this problem we considered $N = 2$ weakly asymmetric states; that is the evolution of initial conditions near integrable symmetric solutions. This problem is directly related to the stability of symmetric solutions, and we showed that symmetric states are linearly stable to exponential normal modes $e^{\gamma t}$. However, the Floquet stability problem is degenerate and there is a linear in time algebraic instability. That is, the relative position

of a hole and clump weakly asymmetric state grows linearly in time. An exception to this is the case of weakly asymmetric shearless solutions which are neutrally stable.

Whether or not this algebraic instability is enough to destroy the coherence of the state depends on nonlinear effects. Here we presented $N = 2$ and $N \to \infty$ kinetic numerical results showing the existence of weakly asymmetric coherent states. In this case, the linear in time algebraic instability leads to a quasiperiodic time evolution of the mean field.

The other problem addressed in this paper is related to the issue of "violent" mixing of far from equilibrium phase space structures. The nontrivial time evolution of the mean field can lead to hyperbolic-elliptic bifurcations in the phase space, and this bifurcations can lead to the rapid mixing of phase space structures. This mechanism is self-consistent as the particles evolve in a mean-field wave whose evolution depends on all them. The constraint imposed by putting initially holes and clumps symmetrically opposed in the wave frame tends to prevent the frequency chirping of the wave. Under this condition, the system has been shown to exhibit a bifurcation in terms of the total momentum of the wave-particle system. Below the threshold, the wave-particle system cannot sustain phase space dipole-like inhomogeneities inside the wave resonance and violently reacts to recover frequency chirping. Above the momentum threshold, the system formed by a bunch of holes coupled to a bunch of clumps is stabilized by parametric effects. We expect the 'violent relaxation' phenomenology to be fully relevant also in comparable dissipative models, provided the dissipative time scale is small compared to the initial rotation time (trapping period).

VI. ACKNOWLEDGEMENTS

MCF gratefully acknowledges the hospitality of the Fusion group at ORNL and fruitful discussions with Y. Elskens, F. Leyvraz and S. Ruffo. MCF thanks European Commission for support through a Marie Curie individual fellowship Contract No HPMFCT-2000-00596 and the US Department of Energy for support. This work was sponsored by the Oak Ridge National Laboratory, managed by UT-Battelle, LLC, for the U.S. Dept. of Energy under

contract DE-AC05-00OR22725.

---

[1] T. M. O'Neil, J. H. Winfrey and J. H. Malmberg, Phys. Fluids **14**, 1204 (1971).

[2] I. N. Onischenko *et al.*, JETP Lett. **12**, 281 (1970).

[3] J. L. Tennyson, J. D. Meiss and P. J. Morrison, Physica D **71** , 1 (1994).

[4] D. del-Castillo-Negrete, Phys. Lett. A **241**, 99 (1998).

[5] D. del-Castillo-Negrete, Phys. Plasmas **5**, 3886 (1998).

[6] M. Antoni, Y. Elskens, and D. F. Escande, Phys. Plasmas **5**, 841 (1998).

[7] M.-C. Firpo and Y. Elskens, J. Stat. Phys. **93**, 193 (1998); Phys. Scripta **T75**, 169 (1998).

[8] D. F. Escande, S. Zekri and Y. Elskens, Phys. Plasmas **3** , 3534 (1996).

[9] M.-C. Firpo and Y. Elskens, Phys. Rev. Lett. **84**, 3318 (2000).

[10] D. del-Castillo-Negrete, Physica A **280**, 10 (2000).

[11] D. del-Castillo-Negrete, CHAOS **10**, 75 (2000).

[12] D. del-Castillo-Negrete and M.-C. Firpo, CHAOS **12** , 496 (2002).

[13] N. J. Balmforth, S. L. Smith and W. R. Young, J. Fluid Mech., **10**, 95-133 (2001).

[14] N. J. Balmforth and C. Piccolo, J. Fluid Mech. **449**, 85-114 (2001).

[15] D. Farina, F. Casagrande, U. Colombo and R. Pozzoli, Phys. Rev. E, **49**, 1603-1609 (1994).

[16] M. Antoni and S. Ruffo, Phys. Rev. E **52**, 2361 (1995).

[17] V. Latora, A. Rapisarda, and S. Ruffo, Physica D, **131**, 38 (1999).

[18] J. Barre, T. Dauxois, and S. Ruffo, Physica A **295**, 254-60 (2001).

[19] H. L. Berk, B. N. Breizman, J. Candy, M. Pekker and N. V. Petviashvilli, Phys. Plasmas **6**, 3102 (1999).

[20] P. Mineau, M. R. Feix and J.-L. Rouet, Astron. Astrophys. **228**, 344 (1990).

[21] D. A. Schecter, D. H. E. Dubin, K. S. Fine, and C. F. Driscoll, Phys. Fluids **11**, 905-914, (1999).

[22] D. del-Castillo-Negrete, J. M. Greene and P. J. Morrison, "Area preserving nontwist maps: periodic orbits and transition to chaos", Physica D **91**, 1 (1996).

[23] J. E. Howard and J. Humpherys, Physica D **80**, 256 (1995).

[24] J. R. Cary and I. Doxas, J. Comput. Phys. **107**, 98 (1993); J. R. Cary *et al.*, Phys. Fluids B **4**, 2062 (1992); I. Doxas and J. R. Cary, Phys. Plasmas **4**, 2508 (1997).

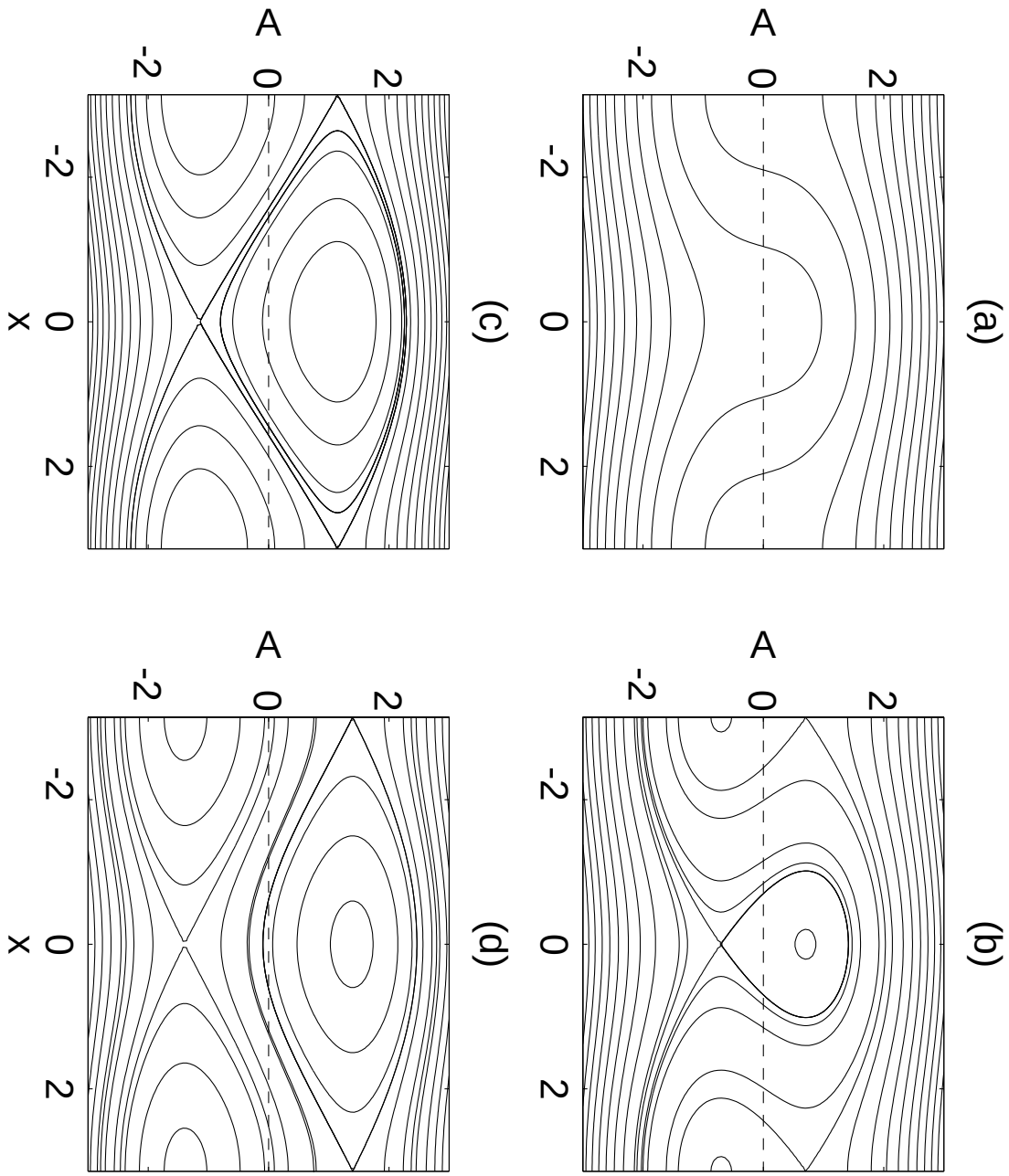

FIG. 1.

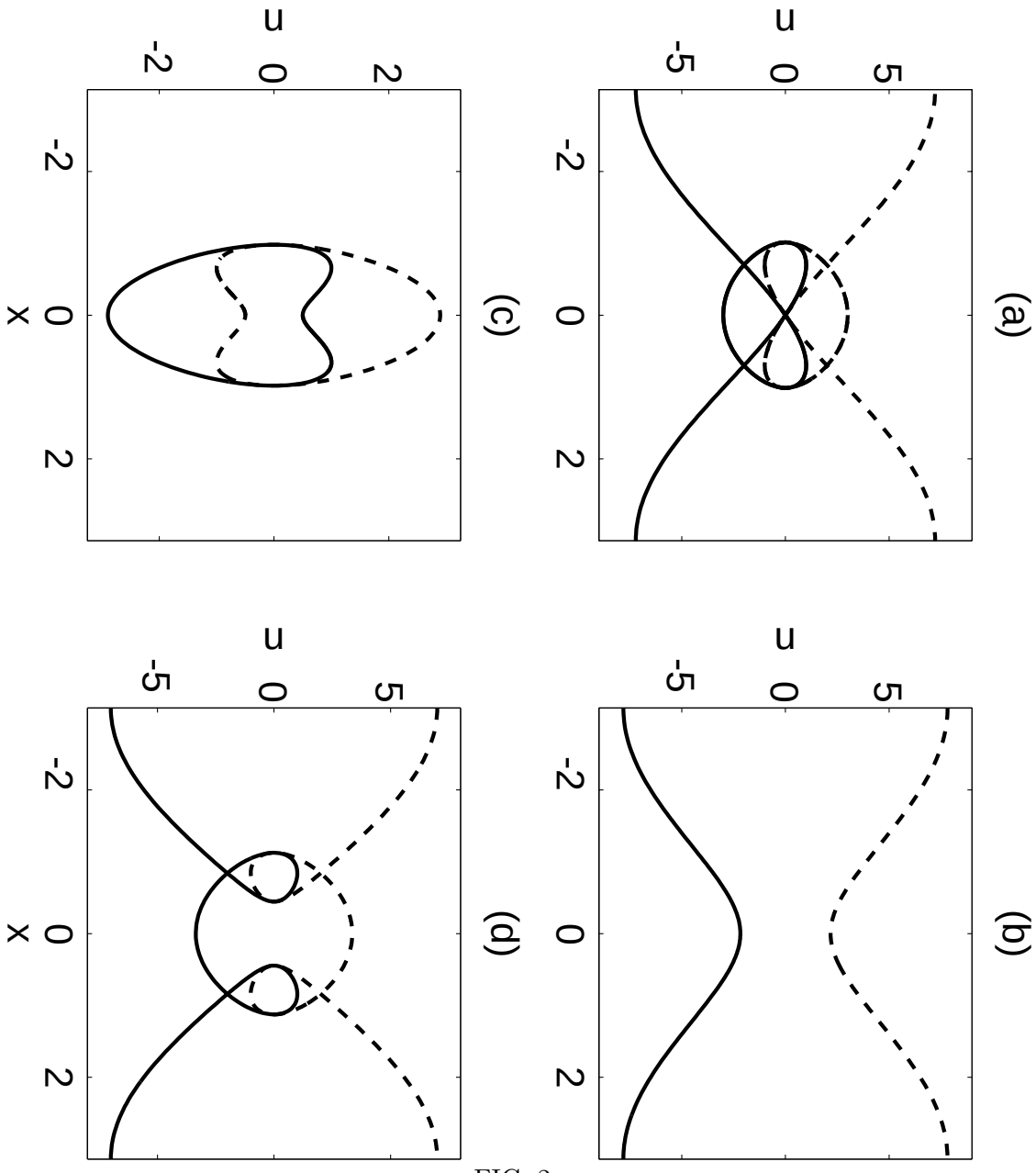

FIG. 2.

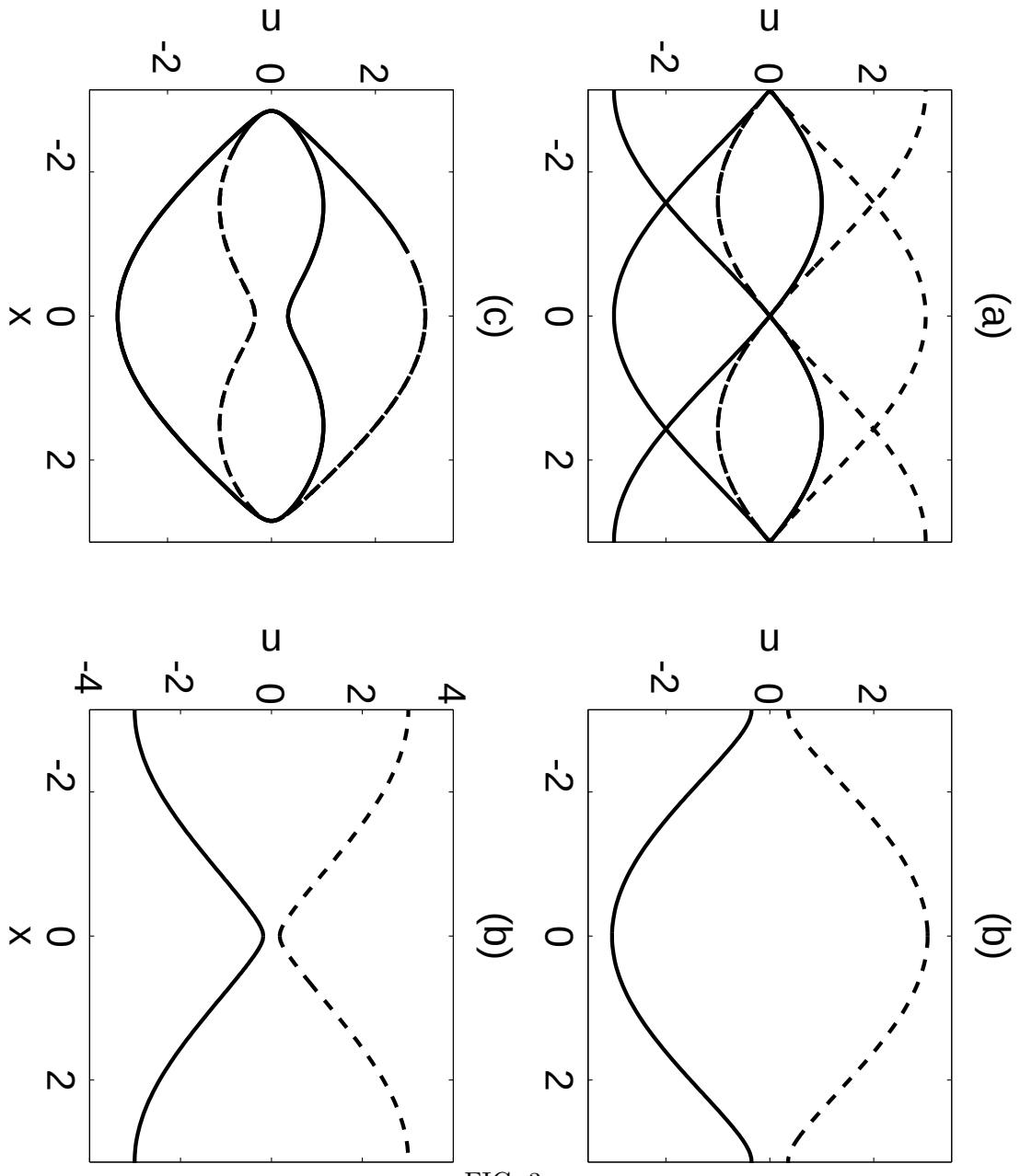

FIG. 3.

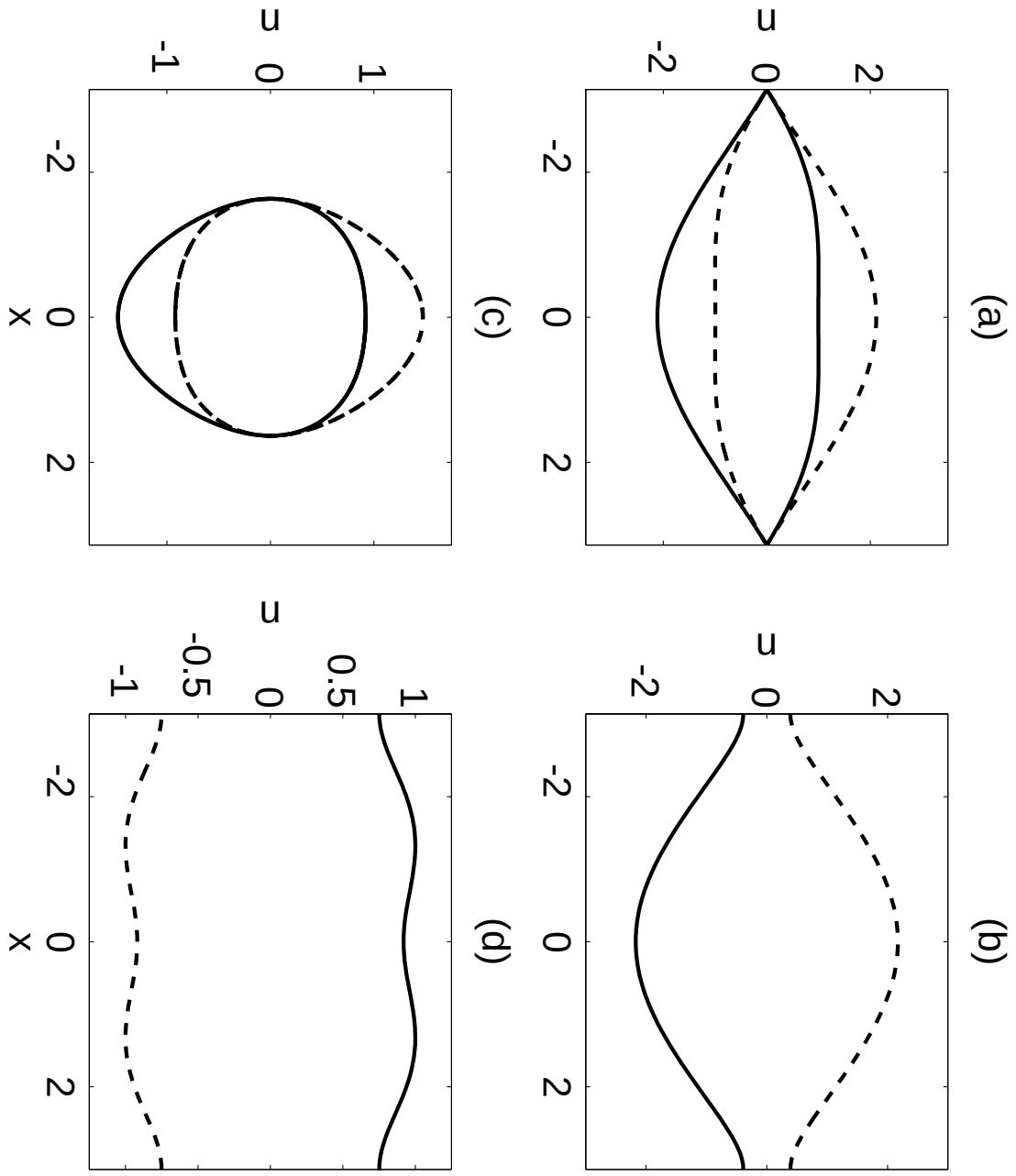

FIG. 4.

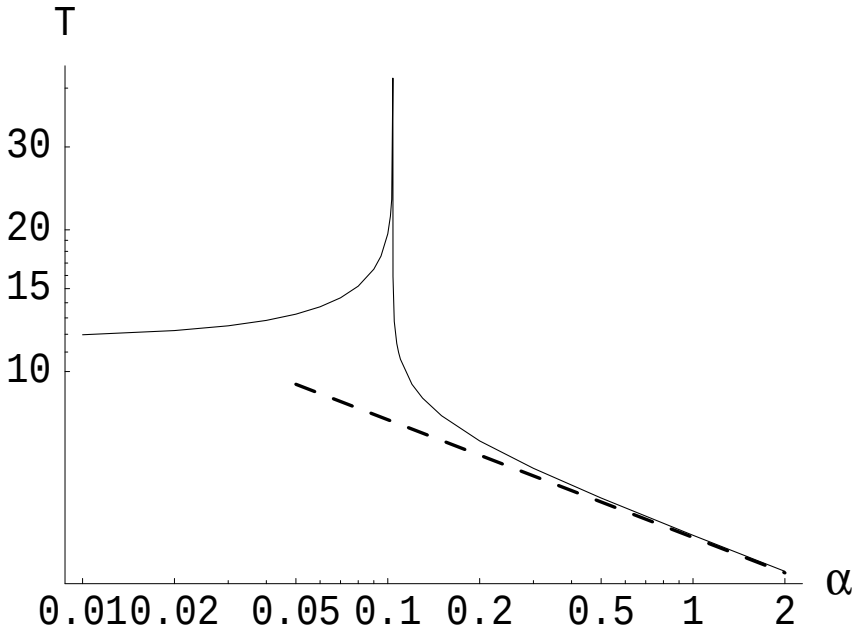

FIG. 5.

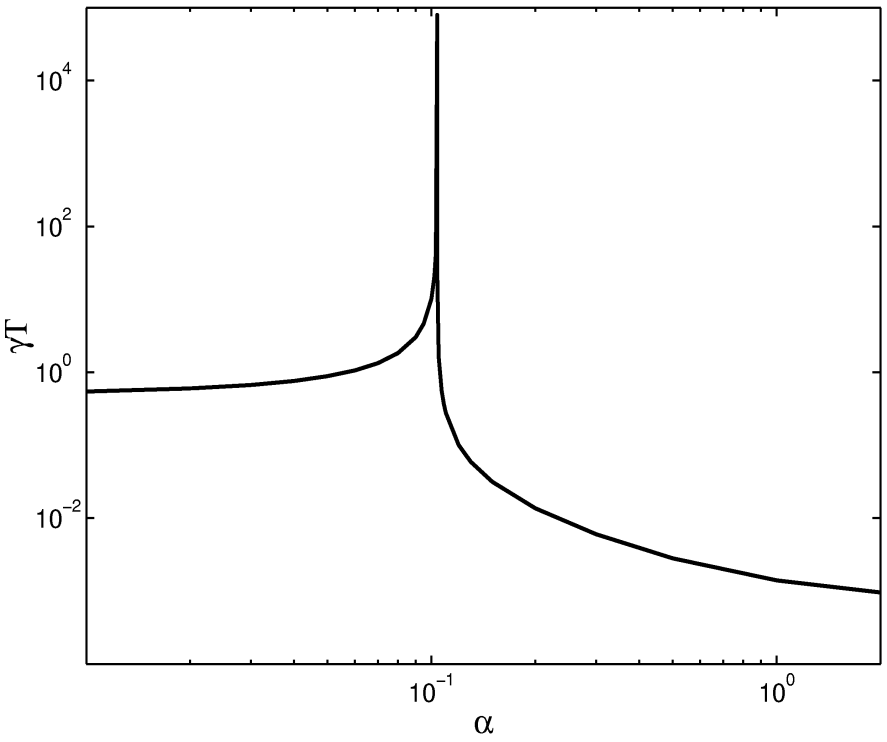

FIG. 6.

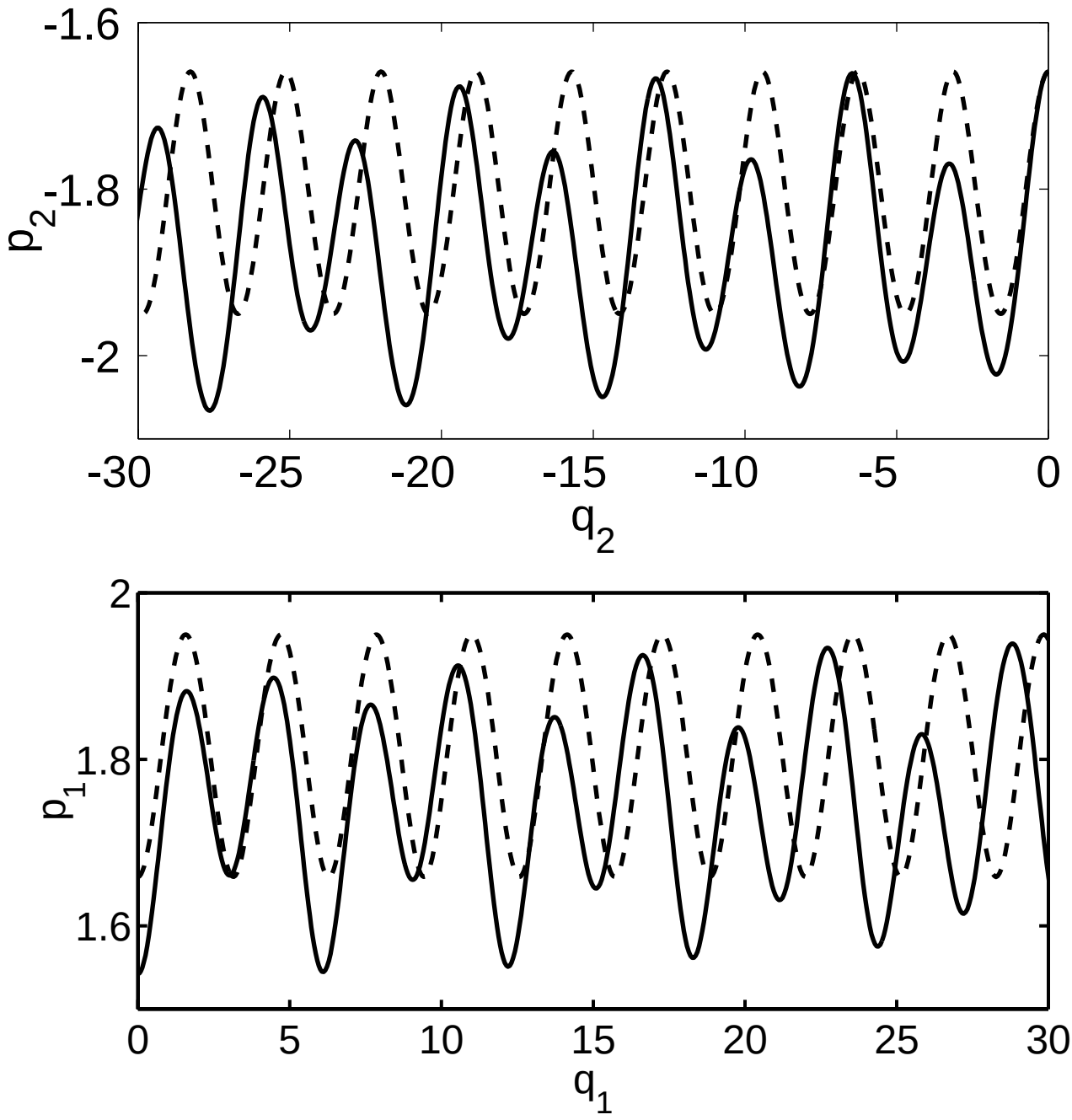

FIG. 7.

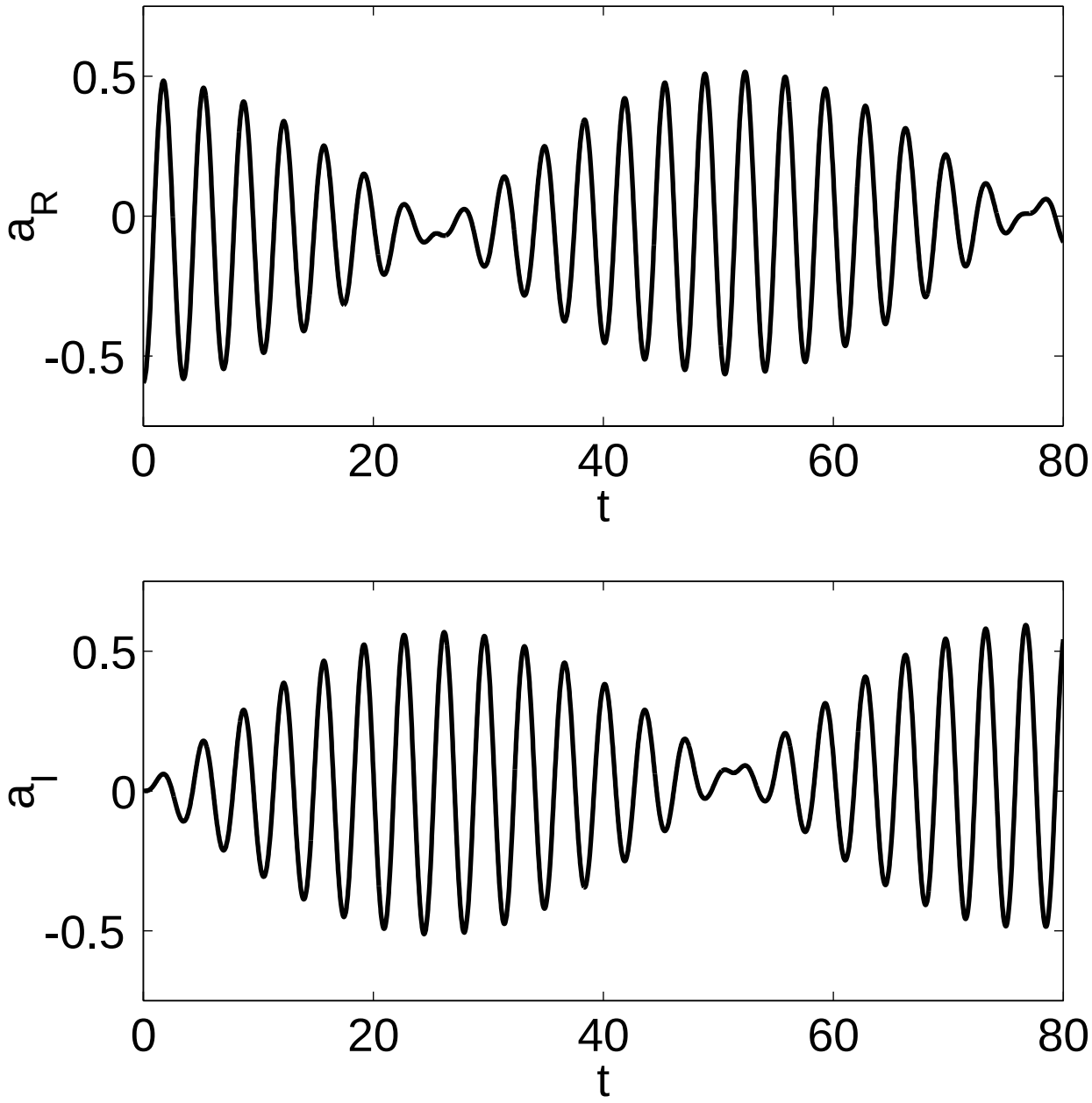

FIG. 8.

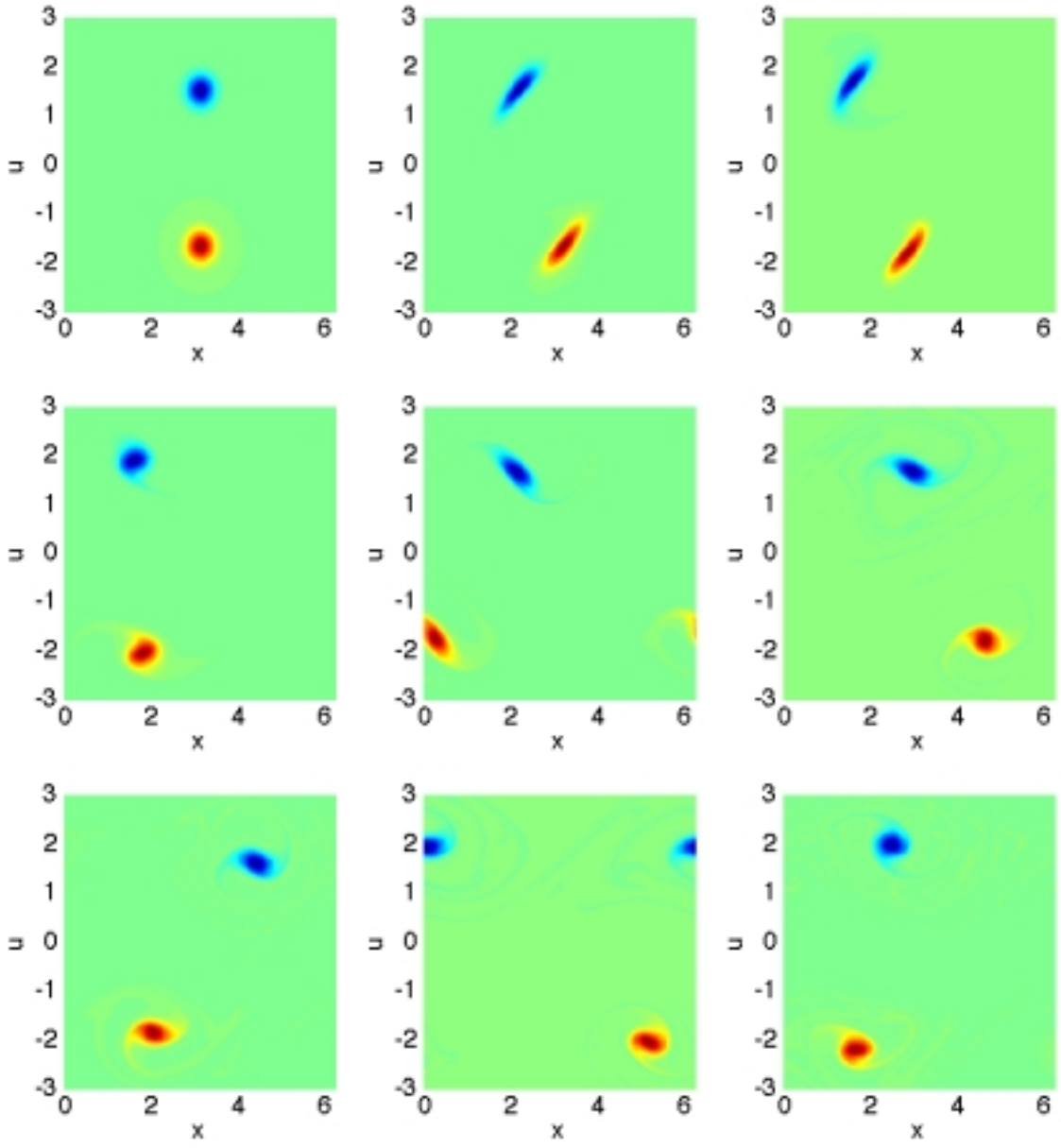

FIG. 9.

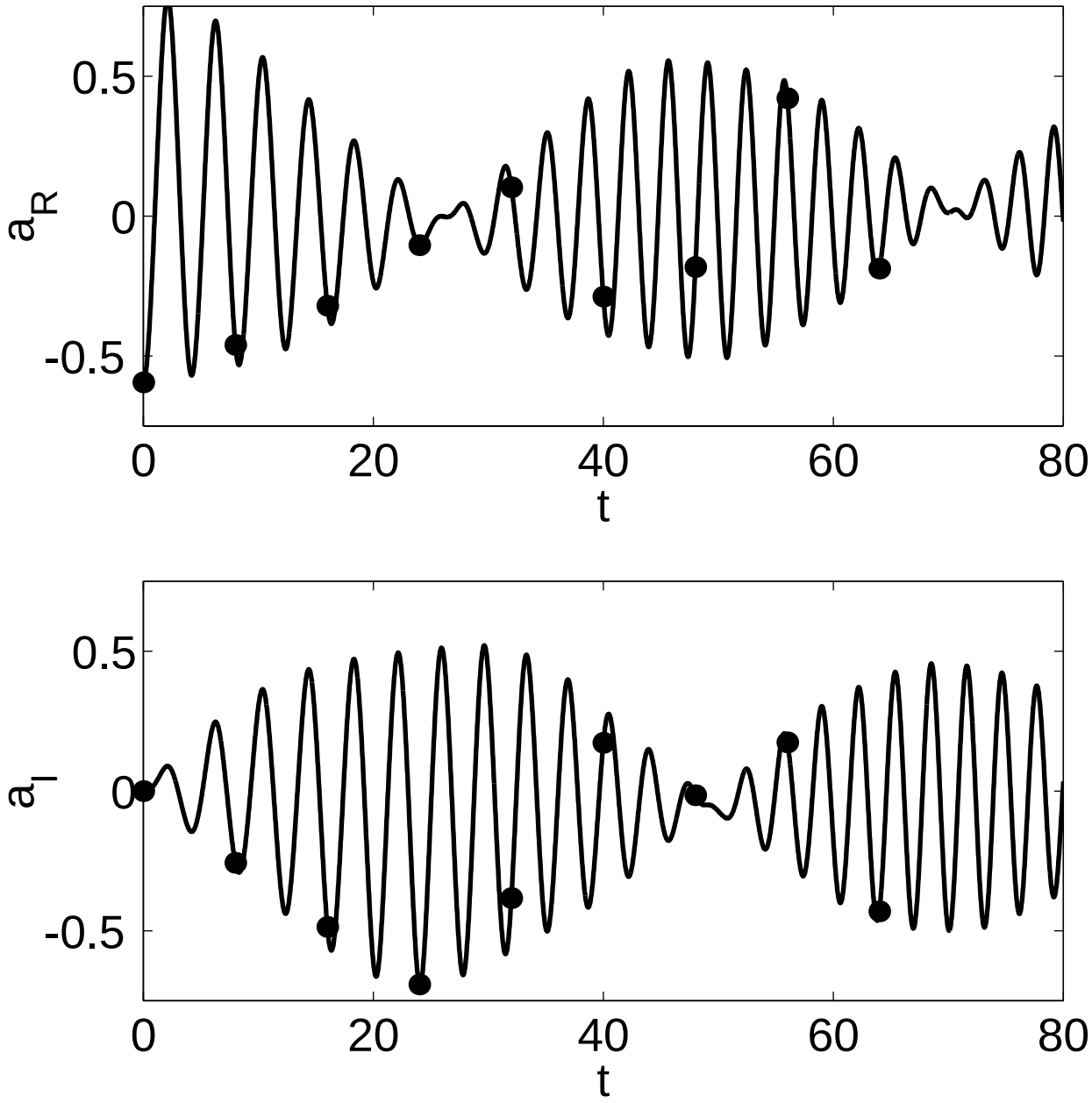

FIG. 10.

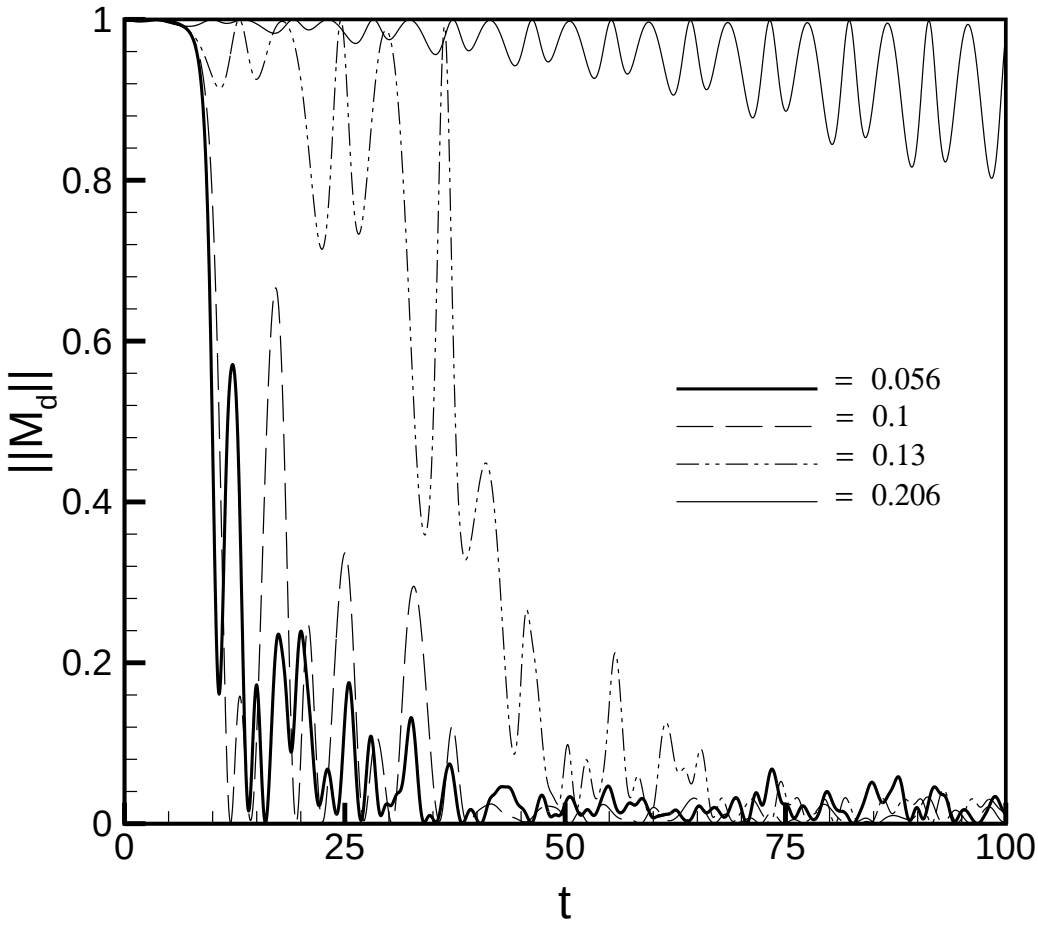

FIG. 11.

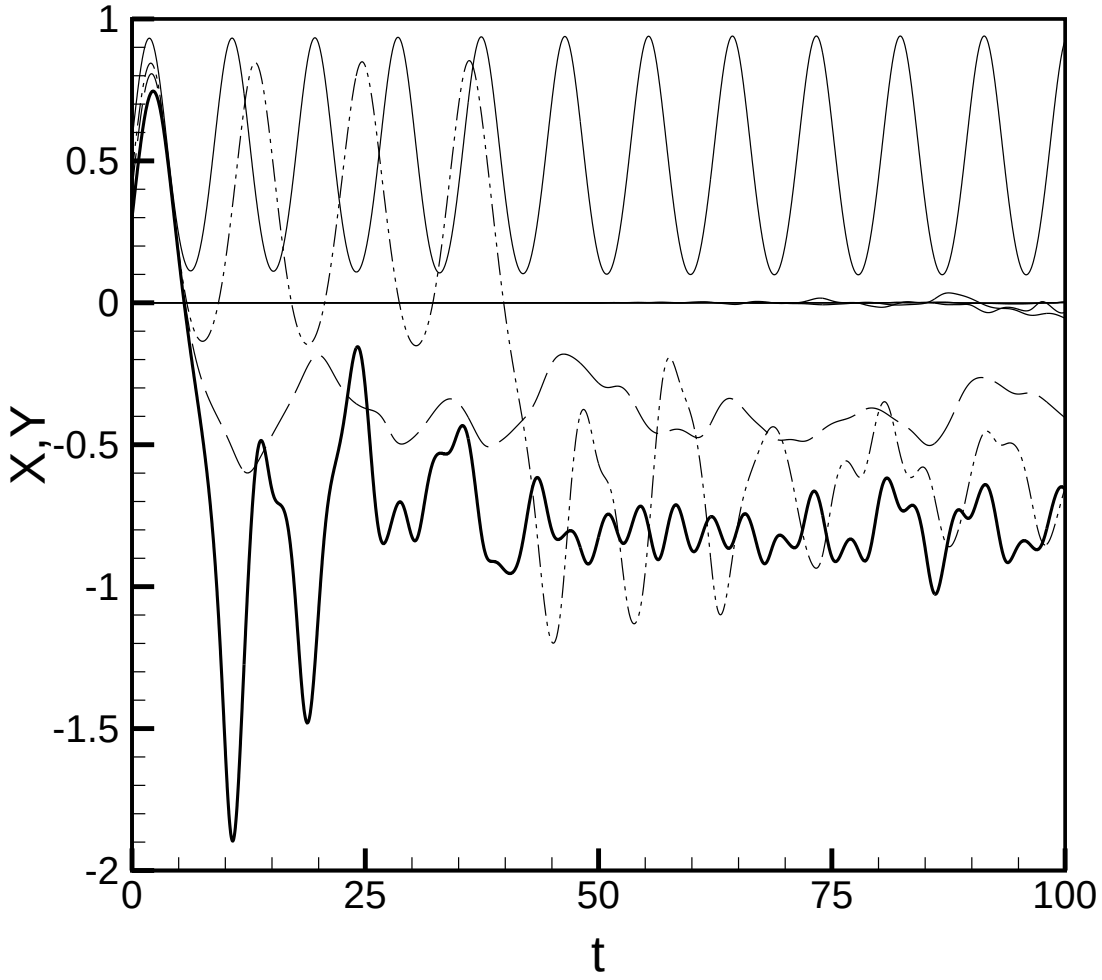

FIG. 12.

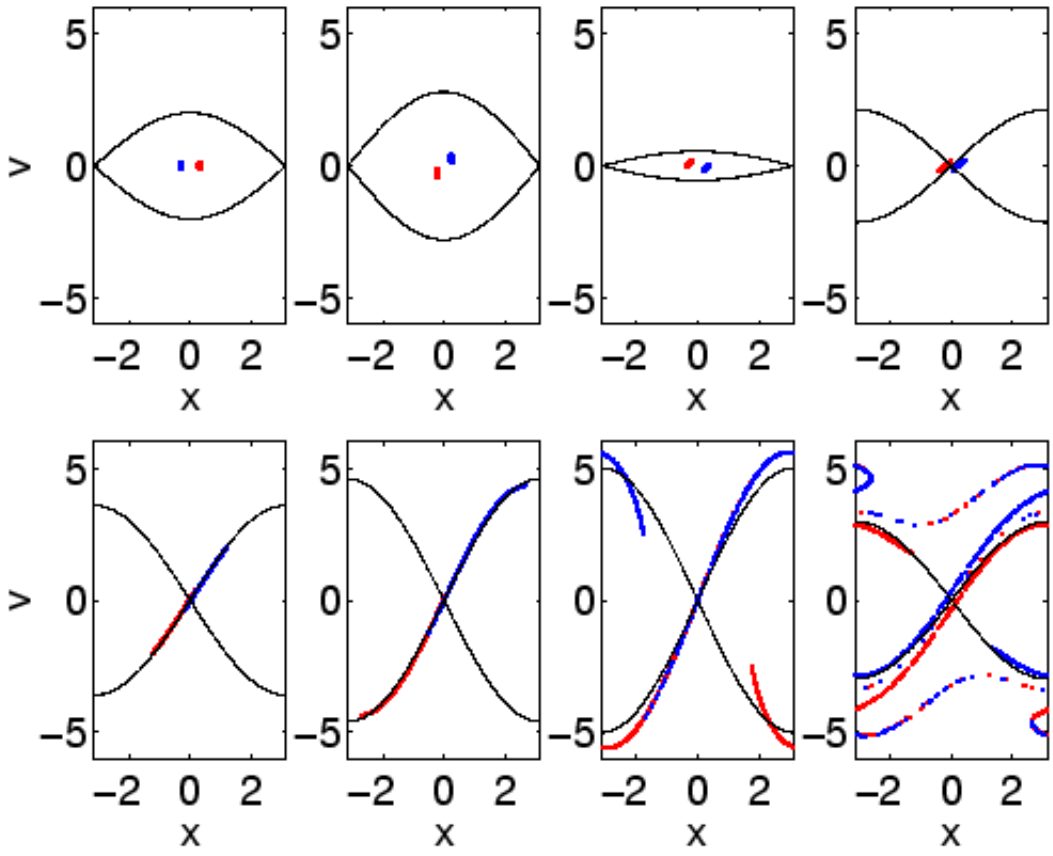

FIG. 13.

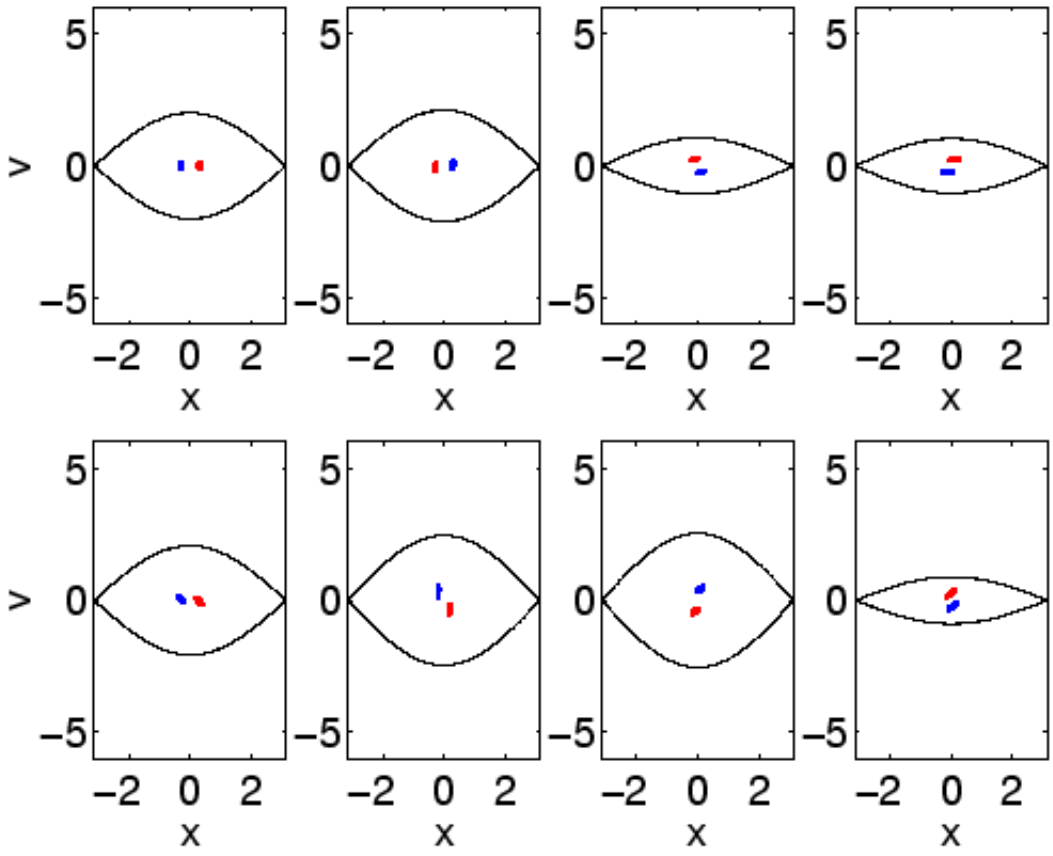

FIG. 14.

FIGURE CAPTIONS

FIG. 1. Contour plots of the symmetric dipole, reduced Hamiltonian in Eq. (18) for: (a) $\alpha = -0.2$, (b) $\alpha = 0.5$, (c) $\alpha = (3/2)^{2/3}$, and (d) $\alpha = 1.95$. In (a) there are no fixed points, case (c) corresponds to the separatrix reconnection threshold, case (b) shows the homoclinic topology and case (d) the heteroclinic topology. Figures 2, 3, and 4 show different hole-clump orbits in the (x, u) phase space corresponding to the different topologies shown in (b), (c) and (d) respectively. Orbits crossing the dashed line $A = 0$ give rise to hyperbolic-elliptic bifurcations.

FIG. 2. Symmetric hole-clump, pair orbits in the (x, u) phase space corresponding to the homoclinic topology in the (x, A) phase space with $\alpha = 0.5$ (same value as that used in Fig. 1-(b)). Orbits corresponding to holes are shown with dashed curves and those corresponding to clumps are shown with solid curves. Panel (a) shows the trajectories corresponding to the lower branch of the separatrix, and panels (b) and (c) show examples of untrapped and trapped trajectories respectively with initial conditions $(x_0, A_0) = (\pi, -2.1)$ and $(0, -0.5)$. Panel (d) shows an example of a loop trajectory between the upper and lower branches of the separatrix with initial condition $(\pi, -2)$.

FIG. 3. Symmetric hole-clump pair orbits in the (x, u) phase space corresponding to the reconnection topology in the (x, A) phase space with $\alpha = (3/2)^{2/3}$ (same value as that used in Fig. 1-(c)). Orbits corresponding to holes are shown with dashed curves and those corresponding to clumps are shown with solid curves. Panel (a) shows the trajectories corresponding to the separatrices, panels (b) and (d) show examples of untrapped trajectories with initial conditions $(x_0, A_0) = (0, 2.3)$ and $((0, -1.24)$, and (c) and example of a trapped trajectory with $(0, -0.94)$.

FIG. 4. Symmetric hole-clump pair orbits in the (x, u) phase space corresponding to the heteroclinic topology in the (x, A) phase space with $\alpha = 1.95$ (same value as that

used in Fig. 1-(d)). Orbits corresponding to holes are shown with dashed curves and those corresponding to clumps are shown with solid curves. Panel (a) shows the trajectories corresponding to the upper branch of the separatrix, panels (b) and (c) show examples of untrapped and trapped trajectories respectively with initial conditions $(x_0, A_0) = (\pi, 1.65)$ and $(0, 0.40)$. Panel (d) shows an example of a trajectory between the upper and lower branches of the separatrix with initial condition $(-\pi, 0.70)$.

FIG. 5. Period T of the dipole solution with initial conditions $x_d(0) = x_0 = 0.3$ and $v_d(0) = 0$ as a function of α in log-log scale. The dashed line represents the rotation period $2\pi/\omega = \sqrt{2}\pi\alpha^{-1/4}$.

FIG. 6. Product γT as a function of α in log-log scale. The reference integrable dipole solutions obey the same initial conditions as in Fig. 5. The initial values of the perturbation are $\delta z_2(0) = 0.01$ and $\tilde{\mathcal{P}} = 0$.

FIG. 7. Hole-clump phase space orbits corresponding to an $N = 2$ asymmetric state. The initial condition, given in Eq. (50)-(51), corresponds to an asymmetric perturbation of the symmetric shearless orbit. Figure 8 shows the mean field. Panel (a) shows the clump and (b) the hole. In both panel, the solid line is the asymmetric orbit and the dashed line the symmetric shearless orbit.

FIG. 8. Mean field quasiperiodic time dependence of an $N = 2$ asymmetric state. The initial condition, given in Eq. (50)-(51), corresponds to an asymmetric perturbation of the symmetric shearless orbit. Figure 7 shows the hole and clump orbits. Panel (a) shows the real part of the mean field and (b) the imaginary part of the mean field.

FIG. 9. Hole-clump phase space dynamics of a kinetic asymmetric state. The initial condition, given in Eq. (52)-(53), corresponds to an asymmetric perturbation of the symmetric shearless orbit. Figure 10 shows the mean field. The panels show the state of the hole and the clump at the successive times marked in Fig. 10.

FIG. 10. Mean field quasiperiodic time dependence of kinetic asymmetric state. The initial condition, given in Eq. (52)-(53), corresponds to an asymmetric perturbation of the symmetric shearless hole-clump state. Figure 9 shows the hole and clump dynamics in the phase space. Panel (a) shows the real part of the mean field and (b) the imaginary part of the mean field. The dots denote the times at which the solutions in Fig. 9 were plotted.

FIG. 11. Modulus of the order parameter M_d as a function of time for the initial conditions described in paragraph IV B with $N = 782$ hole particles and $N = 782$ initially symmetric clump particles with $\Gamma = 1$. The plots relative to four different values of the initial amplitude are shown, corresponding to $\alpha = 0.056$, 0.1, 0.13 and 0.206.

FIG. 12. Plot of the mean field coordinates X and Y as a function of time for the same values of α as in Fig. 11. The same convention for the styles of lines has been used : the bold solid line is relative to $\alpha = 0.056$, the dashed line to $\alpha = 0.1$, the dot-dashed line to $\alpha = 0.13$ and the solid line to $\alpha = 0.206$. The Y curves almost coincide with the horizontal axis during the run, in agreement with the symmetry constraint.

FIG. 13. Phase space plots in the normalized $(x, v/\omega)$ space for $\alpha = 0.056$ at times $\tau = 0$, 3.5, 5.5, 7, 9, 10, 11 and 15. The number of particles in each initial patch is equal to $N = 782$.

FIG. 14. Phase space plots in the normalized $(x, v/\omega)$ space for $\alpha = 0.206$ at times $\tau = 0$, 3.5, 5.5, 7, 9, 10, 11 and 15 (same times as in Fig. 13). As in Fig. 13, the number of particles in each initial patch is equal to $N = 782$.